Bioinformatics, YYYY, 0–0
doi: 10.1093/bioinformatics/xxxxx
Advance Access Publication Date: DD Month YYYY
Manuscript Category

Bioimage Informatics

NRRS: A re-tracing strategy to refine neuron reconstruction

Yiwei Li[1, 2, #], Shengdian Jiang[1, 2, #], and Lijuan Liu[1, *]

[1] Institute for Brain and Intelligence, Southeast University, 210096, Nanjing, Jiangsu Province, China

[2] School of Computer Science and Engineering, Southeast University, 210096, Nanjing, Jiangsu Province, China

# Equal contribution

* Correspondence: Lijuan Liu (lijuan-liu@seu.edu.cn)

Associate Editor: XXXXXXX
Received on XXXXX; revised on XXXXX; accepted on XXXXX

Abstract

Motivation: In neuroscience, it is highly required to produce precise a digital tracing of complete neural morphology from a whole brain imaging dataset. With the participation of human experts in the reconstruction workflow, the complicated annotation challenge brought by the whole brain scale could be addressed. When there are substantial deviations of reconstructed branches and bifurcation points from the underlying image data, the utility of the entire morphological reconstruction is compromised.

Results: We propose a Neuron Reconstruction Refinement Strategy (NRRS) to tackle the problem mentioned before. Our method partitions neuron morphology reconstruction into fixed-size segments and resolves the deviation problems in two steps. We also build a synthetic dataset to validate the performance. We show that NRRS outperforms existing solutions and can handle most deviation errors. In applying our method to SEU-Allen / BICCN dataset containing over 1800 complete neuron reconstructions, we achieve remarkable improvements in the accuracy of the neuron skeleton representation, the task of radius estimation and axonal bouton detection. Our results demonstrate the critical role of our method in refining neuron morphology reconstruction.

Availability: The source code is freely available at https://github.com/Vaa3D/vaa3d_tools/hackathon/Levy/refinement.

Contact: lijuan-liu@seu.edu.cn

Supplementary information: Supplementary data are available at *Bioinformatics* online.

1 Introduction

Digital tracing or reconstruction (**Meijering, 2010**) of a neural morphology is defined to geometrically model the backbone of neurites with countable topologically connected structure components like 3D spheres or lines segments (**Gillette, 2011**), and stores the coordinate, thickness and graph connectivity information in SWC file (**Stockley, 1993**). The reconstruction is usually produced by manual and automatic tracing **(Liu, 2022; Huang, 2022., Basu，2016; Peng, 2011; Xiao, 2013)** of neurites imaging signals which may not distinctive from the noise background. Followed by a proof editing step **(Meijering, 2010; Peng, 2011)**, also called refinement to keep the raw tracing results exactly fit the centerline of neurites imaging signals. Reconstruction results from these datasets, however, are offset of varying degrees to the actual centerline of the neural skeleton due to the complexity of neural morphology, image quality, the defects of automatic algorithms

Recent advances in whole-brain imaging (**Economo, 2016; Gong, 2016**) and related technologies (**Zeng, 2018; Bria, 2016; Wang, 2019; Peng, 2017**) have derived the building of several complete neuron morphology reconstruction datasets in whole-brain scale, including Janelia Research Campus's 1002 dataset **(Winnubst, 2019)**, SEU-Allen's 1741 dataset **(Peng, 2021)**, and ION's 6357 dataset (**Yan, 2020**). A fine digital tracing and quantities of associated morphological characteristics from a whole brain imaging dataset are highly required for classifying neuronal cells (**Adkins, 2020**), determining the role of single neurons within neuronal circuits **(Peng, 2013)** and electrophysiological simulation of individual neurons (**Zhang, 2017**). Subject to fluctuations in image quality of tera-voxel scale whole-brain datasets, manual editing remains an integral part of the production of gold-standard neuron reconstruction datasets. With human experts involved in the reconstruction workflow, the complex annotation challenges posed by the whole-brain scale are partially resolved. Yet different degrees of deviation at branches and bifurcation points are produced, which in turn decreases the utility of further extraction of fine structures like

dendritic spines and axonal boutons.

To mitigate the deviation of neuron reconstruction and improve efficiency, the in- or post-process refinement step is indispensable in regular non-automatic annotation protocols at the whole brain scale **(Winnubst, 2019; Peng, 2021)**. For an intuitive understanding of the situation, we summarized reconstruction deviations into three major cases **(Figure 1).** Case1 deviations appear at internal inflexion neurites, especially in images with a low signal-to-noise ratio (SNR). Case2 deviations occur at the bifurcation point. Case3 shows 3 to 8 pixels of directional deviations of entire neurites. Deviations like Case1 can be caused by a resample operation to a raw SWC file. Case2 is mainly bought by a halfhearted annotation of a human annotator. Both Case1 and Case2 can also be reached by a tracing algorithm with weak tracing performance to noise. A commonly utilized strategy for handling terabyte-sized whole-brain imaging datasets is created hierarchy. For example, TeraFly organizes large-scale imaging datasets in multiple resolution layers to provide a navigation experience similar to Google Maps. However, simply map tracing results at a low-resolution layer to a high-resolution layer would return unfitted reconstruction (Case3).

Mean Shift (MS), as an algorithm proposed for shifting nodes to the nearest centroid literately **(Comaniciu, 1999)**, is usually applied to refine neurite reconstruction in a local imaging block. One drawback for MS is that a maximum searching distance parameter needs to be provided for constraining the solution space, which is hardly general for a complete neuronal reconstruction crossing thousands of imaging blocks. Another is that MS-based solutions have an error hypothesis that the centroid is on the centerline of the neurite which is not satisfying with whole brain imaging data. Similar solutions like 3D shape restriction mean-shift **(Jiang, 2020)** would lead each processing reconstruction unit, normally a node in SWC file, to a locally optimal position without considering the rationality of the entire fitting results.

Here, we introduce a neuron reconstruction refinement strategy (NRRS) to address the above deviation cases mentioned ahead. Instead of developing a new optimization algorithm for complete neuronal reconstruction, we pay attention to automatic tracing methods which have been extensively studied during the past decade. Those automatic methods internally contain centerline optimization functions which would be perfect for our refinement goal. Therefore, based on this idea, our strategy partitions neuron morphology reconstruction into fixed-size segments and resolves the deviation problems through two steps of neuron tracing. Furthermore, we build a synthetic dataset severed as validation data for quantifying the exact performance. We show that NRRS has the ability to handle most of the defined deviation errors while existing solutions hardly achieve matched performance. In applying our method to the SEU-Allen dataset containing nearly 2000 complete neuron reconstructions, we present large improvements obtained in the accuracy of the neuron skeleton representation, the task of radius estimation and axonal bouton detection. The results demonstrate the indispensability of our strategy in refining neuron morphology reconstruction.

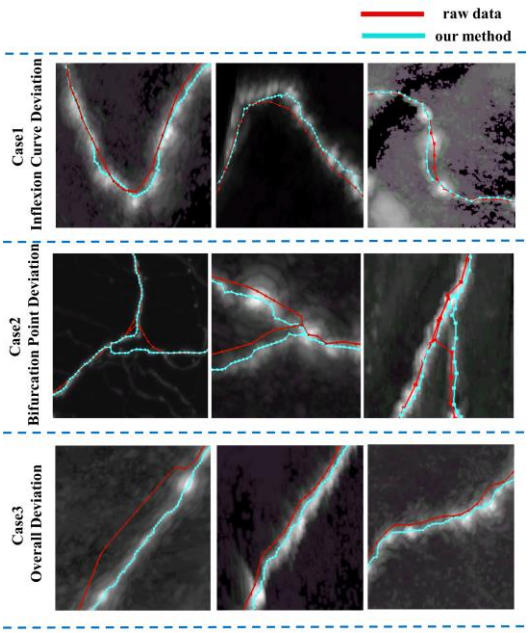

Figure 1. Examples of deviation cases. Case 1: The reconstruction result does not cover the entire bending of the signal. **Case 2:** Reconstruction result fails to find the accurate position of the branch point. **Case 3:** Overall deviations of the reconstruction results.

2 Materials and Methods

2.1 Datasets

The study is being validated and tested around 1741 complete neuron reconstruction dataset (R1741) which is semi-automatically annotated by SEU-ALLEN joint center on 34 mouse brains with the fluorescence micro-optical sectioning tomography fMOST. For precisely quantifying the feasibility of refinement methods, which has not been done by any related studies, we built a synthetic dataset as a test set to reproduce the possible refinement needs in neuron reconstruction. The synthetic dataset contains 1065 local neuron reconstructions and their corresponding image blocks. The generated workflow contains two parts, which are the neuron skeleton formation part and the image formation part (Figure S1). After the workflow, the ground-truth neuron skeleton data, test neuron skeleton data and synthetic neuron images can be obtained. We next randomly sampled 6504 neuron reconstruction 3D blocks (512x512x256, XYZ) from R1741 to further validate the actual performance of our method. We also generated the 178849 MIP **(Sato, 1998)** images ***(512x512, XY)*** of the R1741 to check whether our strategy had introduced potential mistakes.

2.2 Methods

Our method provides a strategy that consists of two re-tracing phases for dealing with the general deviation of neuron reconstruction, the falsely labeled of branching point and the whole brain scale challenge. The overall workflow is shown in Figure 2. With a hypothesis of the total correctness of the annotation of starting point (soma) and terminal points, we limit our refinement on internal nodes of neuron reconstruction. We partition neuron reconstruction into a series of segments with a fixed computer-handled length to ensure the consistency of image quality beforehand. Then, with the goal of optimizing each partitioned segment independently, we make two endpoints an input of a tracing

algorithm, in which can automatically trace an optimal path between those two endpoints and leave the optimization of segment endpoints in the next tracing step.

Details of the procedures are as follows: **I**n the 1st partition step, we partition the neurons into branches according to the bifurcation points, and further partition branches with a length more than 50um into small segments. Then in the 1st re-tracing step, we use graph-augmented deformable model (GD) for the tracing algorithm.1) the graph step: trace a path between the given two points. 2) the deform-step: optimize the morphology of the neuron skeleton by fine-tuning the position of the path nodes traced in the graph step.

The graph step: search the shortest path $\boldsymbol{P}$ between the given start point and endpoint pairs. For graph $\boldsymbol{G = (V, E)}$, $\boldsymbol{V}$ is the set of vertexes in graph and $\boldsymbol{E}$ the set of edges among vertexes. In $\boldsymbol{V}$, each vertex stands for an image voxel. we define the edge weight between vertexes v_0 and v_1 to guarantee that the first re-tracing skeleton passes the image voxels with high intensity. The edge weight as:

$$\boldsymbol{e(v_0, v_1) = \left|\left|v_0 - v_1\right|\right| * \left(\frac{(g_I(v_0)+g_I(v_1))}{2}\right)} \quad \textbf{(1)}$$

Where $\boldsymbol{g_I(.)}$ represents the metric of image voxel intensity. It is defined as:

$$\boldsymbol{g_I = \exp(\lambda_I(1 - I\,(P)/I_{max})^2)} \quad \textbf{(2)}$$

Where $\boldsymbol{I(.)}$ represent the intensity of the image, then we take advantage of the Dijkstra algorithm **(Noto et al., 2000)** to get the shortest path $\boldsymbol{P}$ in graph $\boldsymbol{G}$. $\boldsymbol{\lambda_I}$ is the given constant.

The deform-step: get the initial control point estimation of the deformable model $\{\boldsymbol{C_k}, \boldsymbol{k=1,2\ldots K}\}$ from the path $\boldsymbol{P}$ in the graph-step, which we utilize to define the energy function. Then we apply the local optimization approach to further centralize and refine the skeleton curve $\boldsymbol{C}$. The energy function $\boldsymbol{E}$ is:

$$\boldsymbol{E = \alpha E_{image} + \beta E_{length} + \gamma E_{smoothness}} \quad \textbf{(3)}$$

Where the $\boldsymbol{\alpha}$, $\boldsymbol{\beta}$ and $\boldsymbol{\gamma}$ are the given coefficients of the energy function ($\boldsymbol{\alpha = 1, \beta = \gamma = 0.2}$ in this step).

After the 1st re-tracing step, main body of segment is matched with the center line of neurite signal while two endpoints are still deviated. Therefore, in the second partition step, we partition the results of 1st re-tracing step at the middle points and use the adjacent middle point pairs as the input of the 2nd re-tracing step.

Then, we change the coefficients of the energy functions to achieve the 2nd re-tracing. In the 1st re-tracing step, the most important factor is the image information since the primary goal of is to find the optimal path on the correct signal. Therefore, $\boldsymbol{\alpha}$ should be larger than $\boldsymbol{\beta}$ and $\boldsymbol{\gamma}$. While in the 2nd re-tracing, the start and the end-points of the re-tracing algorithm have already been guaranteed on the correct signal, the smoothness and overall length of the neural skeleton become more important, which means $\boldsymbol{\beta}$ and $\boldsymbol{\gamma}$ should be larger. We set $\boldsymbol{\alpha = \beta = \gamma = 0.5}$. Based on this, a different path is traced through the given points of the 2nd partition and optimized by minimizing the energy function. After the 2nd re-tracing step, the whole skeleton of the reconstructed neuron is refined to the center of the signal.

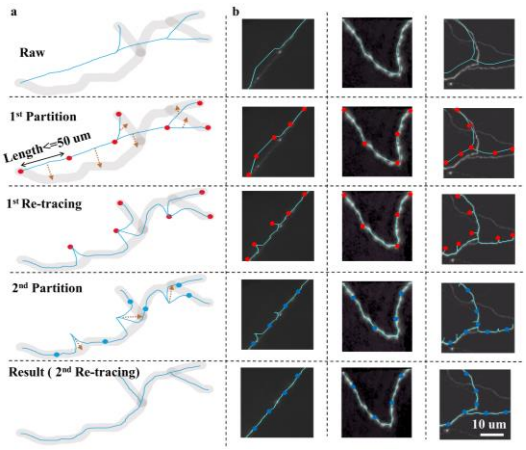

Figure 2. Overall workflow of our refinement strategy. Dots: reconstruction nodes, the connection between which is the neuron skeleton (blue curve) of the segment. Different dot colors indicate results after different partition steps. **a.** Schematic of the four refinement steps: 1) The 1st partition step: break each neuron branch into segments less than 50 μm. 2) The 1st re-tracing step: trace paths between given points. 3) The 2nd partition step: Find the midpoints of the 1st re-tracing path. 4) The 2nd re-tracing step: trace paths between given points. **b.** The processing results of three neurites in different refinement steps. Scale bar: 10um.

3 Experiments and Results

3.1 Validation on Synthetic dataset

For a quantitative assessment of the performance of existing neuron refinement solutions and the superiority of our method, we compare the performance of MS and our method on the synthetic dataset (**Figure 3**). In detail, the first row in **Figure 3a** shows three kinds of image blocks from the synthetic dataset and servers as ground truth data, and the second row is test data consisting of three representative error cases. It is clearly shown in the MS row, MS fails to refine test data to its image signal center and also has bad performance on the refinement of the bifurcation point (Case3). Apparently, our method works well in all three cases, especially in Case3, where our method reaches a more reasonable global optimal path than other methods.

More rigorous conclusions can be drawn from **Figure 3b-g**. The quantities were calculated on the individual synthetic image block and collected from 6504 blocks for bar-plot, including skeleton deviation, bifurcation deviation, radius deviation, intensity deviation, information loss rate and storage size. All the standards are based on the comparison with ground truth. Skeleton deviation represents the average deviation of every reconstructed node. As it is shown in **Figure 3b**, our method outperforms other methods in three aspects. First is a decrease in the average skeleton deviation to 27%. Similarly, our method reduces the bifurcation deviation error to 42%, while other methods only decrease the bifurcation deviation error to 58% (**Figure 3c**). Moreover, our method has the most accurate performance in the extraction of radius and intensity information from neurite signals (**Figure3d-e**).

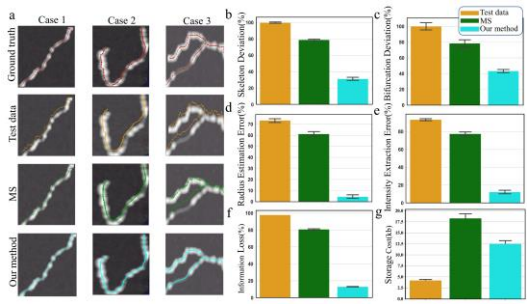

Figure 3. Quantitative validation on a synthetic dataset. a. Examples of the synthetic dataset and the performance of different algorithms. **b-g.** The quantitative comparison between our strategy and other solutions. Our method has a better performance on the statistics validation in solving the deviation of skeleton and bifurcation and can generate more accurate radius estimation and intensity extraction, and with less information loss. Moreover, the reconstruction results refined by our method have a relatively small storage size.

For the reconstruction results of neurons, the essence of the reconstruction result is to extract the necessary information from the image and store it. This process is essentially equivalent to information extraction and compression. Therefore, we further define an information extraction scheme for examining the digital representation ability of different refinement solutions. The information extraction rate is defined as the proportion of the volume covered by the reconstruction result to the actual volume covered by the ground truth signal **(Supplementary Note)**. We resampled the results of different methods to the same interval (2 μm) and then calculated the information extraction rate. It turned out that our strategy only lost about 10% of the information, while other methods lost at least 30% of the information on average. What's more, comparing the storage results of each method when each method achieved the best information extraction rate, it is found that the storage size, which is required to obtain the same information loss rate, of the optimization results of our scheme is only slightly higher than the original data and smaller than the MS algorithm.

3.2 Improvements in Complete Neuron Reconstruction Dataset

To demonstrate the wide applicability of our proposed method, we apply our method to the manually annotated version of the R1741 dataset. The results also showcase the improvements of our refined dataset on biological analysis tasks such as radius estimation and bouton detection.

Examples cropped from the SEU-ALLEN dataset are presented in **Figure 1**. Improvement is obvious after the application of our method. The deviated neuronal skeleton was moved to the center of the signal. Even in the cases of poor signal quality, the results are still excellent. According to Case 2, our method easily made the neuron backbone fit the curved signal perfectly even though the signal is thin and curved. In Case 3, our method found the most suitable bifurcation point on the signal and made the neuron morphology more accurate and reasonable.

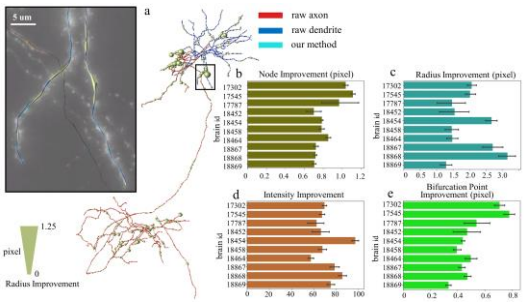

Figure 4. Improvements of our method on the R1741 dataset. a. The example of the improvement in the radius extraction on a whole-brain neuron and the zoom-in view on the place with the biggest radius extraction improvement. **b-e.** The refinement brought by our method can be seen in four aspects, which are node improvement, radius improvement, intensity improvement and bifurcation point improvement.

To quantitatively assess the refinement performance on R1741, we compared four metrics between raw data and refined results including average node change, radius change, intensity change, and bifurcation point change. In **Figure 4a**, the radius of the tube represents the node position change between the raw neuron and the neuron after refinement. The dendrites and the terminal axons have the most displacement. The axon main path has an overall shift as well. As can be seen in **Figure 4b-e**, all brains have an obvious enhancement in four features. For each brain, the average radius has been improved from 0.5 to 1.25 pixels, which indicates some brains might have a better-reconstructed result previously. While for the average distance change, the changes brought by the refinement algorithm seem to be more balanced. The average nodes' refinement distance varies from 1.75 to 2.62 pixels. According to the intensity change, our refinement strategy has brought a boost to the average brightness of reconstructed points per brain from 58 to 96, which shows that our method has shifted the neuron reconstructed results to the right-center of the signal. At last, we calculated the average branch point change. It seems that the branch points did not change a lot from 0.3 to 0.55 pixels. It is the reason that there are many branch points in a whole-brain-level neuron and not every one of the branch points needed to be refined a lot. Therefore, the branch offset may not be obvious enough on the average level. The specific example better illustrates this point.

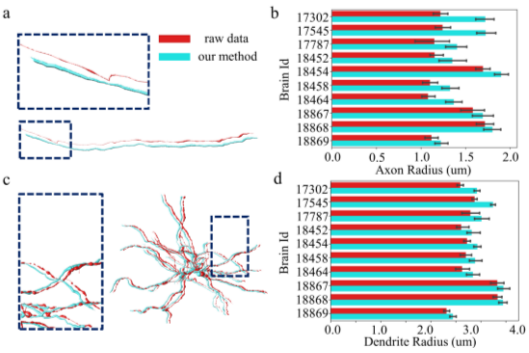

Figure 5. Improvements of radius estimation on axon and dendrite data. a. The improvement of the axon radius measurement after refinement. **b.** Statistical results demonstrate that our method achieves better radius results on over 1400 neurons in ten whole-brain images. **c.** Dendrite radius measurement result also has a better performance. **d.** Statistical results prove that our refinement method has brought an

obvious promotion in the dendrite radius.

We estimated the axon and dendrite radius of the R1741 dataset (Figure 5). The statistical result shows that nearly every brain's average axon radius has increased by 0.15 μm. For brain 17302 and 17545, the increase of the average axon radius comes at the peak of 0.5 μm. According to neural dendrites, the deviation usually happens on the terminal branches. After the refinement of our method, the dendrite radius of each brain is promoted by 0.1~0.3 μm on average. Based on manual judgment and quantitative statistics, our method truly can bring a better effect on radius estimation.

3.3 Improvements in Axonal Bouton Detection

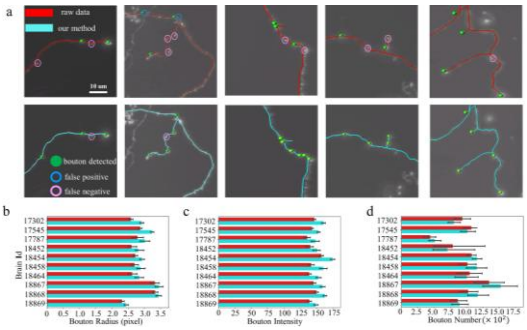

Figure 6. Improvements in whole brain axonal bouton generation. Red line: raw neuron reconstruction results. Blue line: neuron reconstruction results refined by our method. **a.** Our method increases the precision of bouton extraction**. b-d.** Our method extracts the bouton features more accurately and obtains better results on the bouton detection task. The false positive rate increases and the false negative rate decreases.

To showcase our method's performance, we applied our protocols to the task of axonal bouton generation. Axonal bouton usually locates along the axonal signal, and visually has a bigger radius and is brighter than axon in light microscopy data. For this reason, researchers use the radius and intensity information of the axon to determine the position of the potential bouton. We applied the bouton Detection function on Vaa3d **(Jiang, 2022)** on the SEU-ALLEN dataset and cropped 305 images to check the results of bouton detected from the neuron skeleton before and after refinement. Examples can be seen in **Figure 6a**. raw neuron skeletons have lots of false positives and false negatives. While after refinement, because of the more accurate estimation of axon radius, the bouton detection results became more rigorous. We also quantified the boutons extracted from 1741 neurons, including bouton radius, bouton intensity, and bouton number. Both the average bouton radius and bouton intensity are improved. As for the bouton number, statistical results show that the number of boutons extracted for some brains decreases. This is because after the optimization of our method, not only can the originally missed boutons be extracted, but also the detected erroneous boutons can be greatly reduced. In conclusion, our method made the bouton detection task more accurate.

4 Conclusion and Discussion

In this investigation, we proposed a two-step re-tracing strategy, called NRRS, to optimize neuron skeleton reconstruction in the digitalization of neurites. The main goal of our work is to implement a fairly general method not only for partial neuron reconstruction but for dealing with the 'big data' challenge brought by the whole brain scale, we adopted serval specific treatments. The first one is a partition of neuron reconstruction so that it can be processed by current computing hardware and refinement of each partitioned segment would not be affected by the changes in image quality. The second one is the re-tracing idea for optimizing varying degrees of reconstruction deviation. Those treatments make our work outperform existing refinement solutions in either inflexion deviation scenes or entire deviation scenes. In particular, our work has achieved a pretty well performance on refining bifurcation points, which haven't been considered by any other refinement solutions.

In the validation part, previous studies use the visual inspection as the main tactic to validate the refinement performance, which is obviously unrealistic for the ever-growth interest in complete neuron reconstruction at whole-brain scale. Our work, for the first time, formulates a canonical form for the quantitative assessment of the performance of refinement methods and generate a synthetic dataset for validation. Moreover, validating with the same workflow will greatly improve the speed of refinement works in the development phase and benchmark test in comparison.

We showcase the power of our refinement strategy on the SEU-ALLEN whole brain neuron reconstruction dataset, which is the largest complete neuron morphology reconstruction to date. Our strategy decreases the deviation error to less than 6.8% without sacrificing too much storage size. In using a refined version of this dataset, improvements can be obviously noticed in radius estimation, image intensity extraction and axonal bouton detection.

The limitations of present works naturally include two parts, the applicability of the tracing algorithm used in the re-tracing step and the correctness of reconstructed terminal points. In detail, the GD algorithm, here we used in this manuscript, is designed to get a path with less defined cost, in which different parameter groups for the cost function may output various optimized path. One set of parameters can hardly reach a reasonable path for all the situation occurred in whole brain scale. Therefore, one thing needs to be further investigated is adaptive setting of parameters. Another thing needs to be settled is current version cannot refine the tract closed to soma and neural terminal, since our hypothesis is absolutely correct of soma and neural terminal point. A pre-refine of reconstructed soma and neural terminal could further promote the entire refinement of neuron reconstruction.

Our method is implemented as a C++ plugin in Vaa3d system**.** The refinement time cost for a 2-megabyte neural reconstruction is about 3 minutes on a Linux workstation with Intel(R) Xeon(R) Gold 6132 CPU. And the processing can be tremendously speedup by parallelization of the re-tracing step, which is highly useful in largely production of neuron reconstruction.

Availability and implementation

The study is conducted based on the open sourced Vaa3D platform, which is available on the GitHub (https://github.com/Vaa3D). The proposed refinement method is implemented as a Vaa3D plugin and the source code to refine neuron skeleton reconstruction from local image data and whole brain level image dataset are available under the

repository of vaa3d_tools/hackathon/Levy/refinement. The original fMOST images of mouse brains can be found at the BICCN's Brain Image Library (BIL) (https://www.brainimagelibrary.org). The synthetic dataset is shared on GitHub (vaa3d_tools/hackathon/Levy/refinement at master · Vaa3D/vaa3d_tools (github.com)).

Authors' contributions

L.L. initiated this study as a part of quality control in the large-scale neuron morphology data production workflow of the SEU-ALLEN / BICCN datasets, provided necessary resources of this study and managed the overall quality of the project. Y.L. and S.J. co-developed the refinement methods, the generation of synthetic dataset and writing of manuscript.

Acknowledgements

This work has been funded by Southeast University (SEU) to support the Full Neuronal Reconstruction Platform and a MOST (China) Brain Research Project, "Mammalian Whole Brain Mesoscopic Stereotaxic 3D Atlas" (2022ZD0205200, 2022ZD0205204).. We thank Sujun Zhao and Peng Xie for the assistance in manuscript writing and organization. We thank Ye Zhong, Yuning Hang, Gaoyu Wang, Yuanyuan Song and Yufeng Liu for the visual inspection works on whole brain level datasets.

Conflicts of interest

The authors have no competing interests.

Reference:

Adkins, R. S., Aldridge, A. I., Allen, S., Ament, S. A., An, X., Armand, E., ... & Mitra, P. P. (2020). A multimodal cell census and atlas of the mammalian primary motor cortex. *BioRxiv*.

Allen cell types database. allen institute for brain science. http://celltypes.brain-map.org/data

Basu,S. *et al.* (2016) Neurite Tracing with Object Process. *IEEE Transactions on Medical Imaging*, **35**, 1443–1451.

Bentley, J. L. (1980). Multidimensional divide-and-conquer. *Communications of the ACM*, *23*(4), 214-229.

Bria, A., Iannello, G., Onofri, L., & Peng, H. (2016). TeraFly: real-time three-dimensional visualization and annotation of terabytes of multidimensional volumetric images. *Nature methods*, *13*(3), 192-194.

Comaniciu, D., & Meer, P. (1999, September). Mean shift analysis and applications. In *Proceedings of the seventh IEEE international conference on computer vision* (Vol. 2, pp. 1197-1203). IEEE.

Donohue, D. E., & Ascoli, G. A. (2011). Automated reconstruction of neuronal morphology: an overview. *Brain research reviews*, *67*(1-2), 94-102.

Economo, M. N., Clack, N. G., Lavis, L. D., Gerfen, C. R., Svoboda, K., Myers, E. W., & Chandrashekar, J. (2016). A platform for brain-wide imaging and reconstruction of individual neurons. *Elife*, *5*, e10566.

Feng, L., Zhao, T., & Kim, J. (2015). neuTube 1.0: a new design for efficient neuron reconstruction software based on the SWC format. *eneuro*, *2*(1).

Gala, R., Lebrecht, D., Sahlender, D. A., Jorstad, A., Knott, G., Holtmaat, A., & Stepanyants, A. (2017). Computer assisted detection of axonal bouton structural plasticity in in vivo time-lapse images. *Elife*, *6*, e29315.

Gillette, T. A., Brown, K. M., Svoboda, K., Liu, Y., & Ascoli, G. A. (2011). DIADEMchallenge. Org: a compendium of resources fostering the continuous development of automated neuronal reconstruction.

Gong, H., Xu, D., Yuan, J., Li, X., Guo, C., Peng, J., ... & Luo, Q. (2016). High-throughput dual-colour precision imaging for brain-wide connectome with cytoarchitectonic landmarks at the cellular level. *Nature communications*, *7*(1), 1-12.

Huang, Q., Cao, T., Zeng, S., Li, A., & Quan, T. (2022). Minimizing probability graph connectivity cost for discontinuous filamentary structures tracing in neuron image. *IEEE Journal of Biomedical and Health Informatics*.

Jiang, S., Wang, Y., Liu, L., Ding, L., Ruan, Z., Dong, H. W., ... & Peng, H. (2022). Petabyte-scale multi-morphometry of single neurons for whole brains. *Neuroinformatics*, 1-12.

Jiang, S., Pan, Z., Feng, Z., Guan, Y., Ren, M., Ding, Z., ... & Li, A. (2020). Skeleton optimization of neuronal morphology based on three-dimensional shape restrictions. *BMC bioinformatics*, *21*(1), 1-16.

Liu,Y., Wang, G., Giorgio A., Zhou J.,...&Liu, L.,(2022). Neuron Tracing from Light Microscopy Images: Autom ation, Deep Learning, and Bench Testing,*Bioinformatics,* under review.

Meijering, E. (2010). Neuron tracing in perspective. *Cytometry Part A*, *77*(7), 693-704.

Noto, M., & Sato, H. (2000, October). A method for the shortest path search by extended Dijkstra algorithm. In *Smc 2000 conference proceedings. 2000 ieee international conference on systems, man and cybernetics.'cybernetics evolving to systems, humans, organizations, and their complex interactions'(cat. no. 0* (Vol. 3, pp. 2316-2320). IEEE.Oztas, E. (2003). Neuronal tracing. *Neuroanatomy*, *2*(2), 5.

Peng, H., Long, F., & Myers, G. (2011). Automatic 3D neuron tracing using all-path pruning. *Bioinformatics*, *27*(13), i239-i247.

Peng, H., Roysam, B., & Ascoli, G. A. (2013). Automated image computing reshapes computational neuroscience. *BMC bioinformatics*, *14*(1), 1-5.

Peng, H., Long, F., Zhao, T., & Myers, E. (2011). Proof-editing is the bottleneck of 3D neuron reconstruction: the problem and solutions. *Neuroinformatics*, *9*(2), 103-105.

Peng, H., Ruan, Z., Atasoy, D., & Sternson, S. (2010). Automatic reconstruction of 3D neuron structures using a graph-augmented deformable model. *Bioinformatics*, *26*(12), i38-i46.

Peng, Hanchuan, et al. "Automatic tracing of ultra-volumes of neuronal images." *Nature methods* 14.4 (2017): 332-333.

Peng, H., Zhou, Z., Meijering, E., Zhao, T., Ascoli, G. A., & Hawrylycz, M. (2017). Automatic tracing of ultra-volumes of neuronal images. *Nature methods*, *14*(4), 332-333.

Peng, Hanchuan, et al. "Morphological diversity of single neurons in molecularly defined cell types." *Nature* 598.7879 (2021): 174-181.

Peng, H., Xie, P., Liu, L., Kuang, X., Wang, Y., Qu, L., ... & Zeng, H. (2021). Morphological diversity of single neurons in molecularly defined cell

types. *Nature*, *598*(7879), 174-181.

Ruder, Sebastian. "An overview of gradient descent optimization algorithms." *arXiv preprint arXiv:1609.04747* (2016).

Ruder, S. (2016). An overview of gradient descent optimization algorithms. *arXiv preprint arXiv:1609.04747*.

Sato, Y., Shiraga, N., Nakajima, S., Tamura, S., & Kikinis, R. (1998). Local maximum intensity projection (LMIP: A new rendering method for vascular visualization. *Journal of computer assisted tomography*, *22*(6), 912-917.

Stockley, E. W., Cole, H. M., Brown, A. D., & Wheal, H. V. (1993). A system for quantitative morphological measurement and electrotonic modelling of neurons: three-dimensional reconstruction. *Journal of neuroscience methods*, *47*(1-2), 39-51.

Wang, X., Tucciarone, J., Jiang, S., Yin, F., Wang, B. S., Wang, D., ... & Huang, Z. J. (2019). Genetic single neuron anatomy reveals fine granularity of cortical axo-axonic cells. *Cell reports*, *26*(11), 3145-3159.

Wang, Y., Li, Q., Liu, L., Zhou, Z., Ruan, Z., Kong, L., ... & Peng, H. (2019). TeraVR empowers precise reconstruction of complete 3-D neuronal morphology in the whole brain. *Nature communications*, *10*(1), 1-9.

Winnubst, J., Bas, E., Ferreira, T. A., Wu, Z., Economo, M. N., Edson, P., ... & Chandrashekar, J. (2019). Reconstruction of 1,000 projection neurons reveals new cell types and organization of long-range connectivity in the mouse brain. *Cell*, *179*(1), 268-281.

Xiao, H., & Peng, H. (2013). APP2: automatic tracing of 3D neuron morphology based on hierarchical pruning of a gray-weighted image distance-tree. *Bioinformatics*, *29*(11), 1448-1454.

Yan, J., Gao, L., Liu, S., Gou, L., Hu, Y., Liu, Y. H., ... & Xu, N. L. (2020). Topographic organization of single-neuron projectome for mouse prefrontal cortex.

Zeng, H. (2018). Mesoscale connectomics. *Current opinion in neurobiology*, *50*, 154-162.

Zhang, X., Liu, S., Zhan, F., Wang, J., & Jiang, X. (2017). The effects of medium spiny neuron morphologcial changes on basal ganglia network under external electric field: A computational modeling study. *Frontiers in computational neuroscience*, *11*, 91.